

THE LOSS-CONE DRIVEN INSTABILITY FOR LANGMUIR WAVES IN AN UNMAGNETIZED PLASMA

R. G. HEWITT and D. B. MELROSE

School of Physics, University of Sydney, Sydney N.S.W. 2006, Australia

(Received 4 September; in revised form 4 December, 1984)

Abstract. Analytic and numerical results are presented for the growth rate of Langmuir waves due to a loss-cone distribution of energetic electrons. The effect of the magnetic field on the wave-particle interaction is ignored, and the resonance condition is described in terms of a resonance hyperboloid in momentum space. The collisional evolution of a distribution of magnetically trapped electrons is followed numerically to show how a 'gap' distribution develops. The growth is most favorable for an intermediate sized loss cone ($\alpha \sim 45^\circ$) and a 'gap' distribution in which the mean energy of the suprathermal electrons is much larger than the thermal energy of the background electrons. It is plausible that loss-cone 'gap' distributions do develop in the solar corona, and that they should lead to second harmonic plasma emission weakly polarized in the x -mode.

1. Introduction

Plasma emission, that is emission at the plasma frequency ω_p and its second harmonic, is thought to be the emission mechanism for most solar radio bursts at meter and decimeter wavelengths. Plasma emission requires the presence of Langmuir turbulence in the source, and only three mechanisms for generating such turbulence seem to be relevant: a streaming instability, an isotropic 'gap' distribution, and a loss-cone instability. For type III bursts and for the herringbone structure in type II bursts there is direct evidence for electron streams and a streaming instability is the accepted mechanism. The absence of evidence for adequate streaming motions in other types of burst suggests that one of the other two mechanisms is relevant.

An isotropic 'gap' distribution (Tidman and Dupree, 1965; Melrose, 1975) can produce a moderately high level of Langmuir turbulence, which is, however, restricted by a relativistic term in the absorption coefficient (Robinson, 1977; Melrose, 1980b, p. 142). As a consequence a 'gap' distribution cannot produce second harmonic plasma emission brighter than 3×10^9 K. At least for some bright emission, e.g. type I bursts and drift pairs, brightness temperatures in excess of this value have been observed, and a 'gap' distribution is inadequate.

These arguments lead one to conclude that a loss-cone instability may be relevant for a variety of solar radio bursts. The specific application discussed most extensively is to decimeter type IV bursts, e.g. Stepanov (1973, 1978), Kuijpers (1974), Benz and Kuijpers (1976), Zaitsev and Stepanov (1975), and the review by Kuijpers (1980). Possible applications to meter-wave bursts have been mentioned by Melrose and Stenhouse (1977), Melrose (1978), and Robinson (1977); a favorable application is to type I bursts (Melrose, 1980c; Benz and Wentzel, 1981). Recently Zaitsev and Stepanov (1983) applied the loss-cone instability to microwave emission from flare kernels.

Our purpose in this paper is to present the results of a systematic study of the properties of the loss-cone driven instability for Langmuir waves in an unmagnetized plasma. In the literature cited above, the loss-cone instability has been treated in a variety of ways; when the magnetic field is neglected (see comments below) it has usually been assumed (a) that the maximum growth is perpendicular to the magnetic field lines, and only growth at this angle is considered, and (b) that the loss-cone has sharp edges. We relax both these assumptions. We also explore the effects of collisions on a given initial distribution (either a hot Maxwellian or a power-law in momentum); it is known that collisions can lead to the formation of a 'gap' distribution (with $\partial f(p)/\partial p > 0$ over a finite range) and it is thought that a 'gap' or a 'plateau' ($\partial f(p)/\partial p \simeq 0$) momentum distribution as well as a loss-cone anisotropy is required to drive the instability (e.g. Kuijpers, 1974; Robinson, 1977).

Our neglect of the magnetic field requires comment. In one sense the magnetic field cannot be neglected because a loss-cone distribution develops only when particles are trapped in a magnetic bottle and those with small pitch angles escape out the ends. Neglecting the magnetic field here is equivalent to assuming (a) that the resonance condition is the Cerenkov condition $\omega - \mathbf{k} \cdot \mathbf{v} = 0$ rather than the Doppler condition $\omega - s\Omega_e/\gamma - k_{\parallel}v_{\parallel} = 0$, and (b) that the only relevant waves are Langmuir waves (with dispersion relation $\omega \simeq [\omega_p^2 + 3k^2V_e^2]^{1/2}$ as in an unmagnetized plasma). These assumptions should be valid for $kv \simeq \omega_p \gg \Omega_e$ provided one is not specifically interested in the Bernstein waves. The complicating effects of magnetic field are expected to be more qualitative than quantitative for $\omega_p \gg \Omega_e$. By this we mean that the growth rates in the magnetized and unmagnetized cases are not greatly different; there are exceptions, however, notably the case of the double resonance (e.g. Zheleznyakov and Zlotnik, 1975; Kuijpers, 1980). Our justification for neglecting the magnetic field here is that the unmagnetized case has not been explored adequately, and that it should be explored before the complicating effects of the magnetic field are taken into account.

In Section 2 we evaluate the absorption coefficient for Langmuir waves due to an axially symmetric distribution of suprathermal electrons; we also develop a geometric interpretation of the resonance condition in terms of a resonance hyperboloid in momentum space, and use this in an Appendix to treat an idealized loss-cone distribution. In Section 3 we discuss the evolution of initial Maxwellian and loss-cone distributions in a trap-plus-precipitation model, showing how a 'gap' distribution develops. Our numerical results for the growth rate are presented in Section 4 and the results are discussed in Section 5.

2. The Absorption Coefficient for Langmuir Waves and Axially Symmetric Electrons

We calculate the absorption coefficient for Langmuir waves under the following assumptions: (i) the background magnetic field is negligible, (ii) the wave dispersion is determined by a dense non-relativistic Maxwellian electron gas (subscript C), and (iii) there

is a low-density axially-symmetric electron distribution with mean energy much greater than the thermal energy.

A. WAVE PROPERTIES

The wave properties for Langmuir waves are well known; we summarize them here to introduce our notation.

The longitudinal part of the dielectric tensor $K^L(k, \omega)$ for an isotropic non-relativistic electron gas with number density n_C , plasma frequency $\omega_p = [e^2 n_C / m \epsilon_0]^{1/2}$ and temperature $T_C = mV^2$ is

$$K^L(k, \omega) = 1 + \frac{\omega_p^2}{k^2 V^2} [1 - \phi(y) + i\sqrt{\pi} y e^{-y^2}] \quad (1)$$

with $y = \omega / \sqrt{2} kV$ and

$$\phi(y) = 2ye^{-y^2} \int_0^y dt e^{t^2}. \quad (2)$$

The dispersion relation $\omega = \omega_L(k)$ is found by solving $\text{Re}[K^L(k, \omega)] = 0$ which reduces to

$$\phi(y) - 1 = \frac{k^2 V^2}{\omega_p^2}. \quad (3)$$

The ratio of electric to total energy (cf. Melrose, 1980a, p. 47) is

$$\begin{aligned} R_L(k) &= \left[\frac{\partial}{\partial \omega} \left\{ \omega \text{Re} K^L(k, \omega) \right\} \right]^{-1} \Big|_{\omega = \omega_L(k)} \\ &= \frac{1}{2} \left(1 - \frac{k}{\omega_L(k)} \frac{d\omega_L(k)}{dk} \right) \simeq \frac{\omega_L^2(k)}{2\omega_p^2}, \end{aligned} \quad (4)$$

where the approximate expression applies for $y \gg 1$. The Landau absorption coefficient is

$$\begin{aligned} \gamma_L(k) &= 2R_L(k) [\omega \text{Im} K^L(k, \omega)]_{\omega = \omega_L(k)} \\ &\simeq \sqrt{\frac{\pi}{2}} \frac{\{\omega_L(k)\}^4}{(kV)^3} \exp \left[-\frac{\{\omega_L(k)\}^2}{2k^2 V^2} \right]. \end{aligned} \quad (5)$$

In the numerical calculations below we have calculated $\omega_L(k)$, $R_L(k)$, and $\gamma_L(k)$ exactly, i.e. without assuming $y \gg 1$. A solution of (3) exists for $y \gtrsim 1.5$.

B. SUPRATHERMAL AXIALLY-SYMMETRIC DISTRIBUTION

Let $f(\mathbf{p})$, with

$$\int d^3\mathbf{p} f(\mathbf{p}) = 1, \quad (6)$$

denote an axially-symmetric distribution of suprathermal electrons with number density n_H . The absorption coefficient for Langmuir waves at an angle θ to the symmetry (z) axis (e.g. Melrose, 1980a, p. 161) reduces to ($\omega = \omega_L(k)$ hereafter)

$$\gamma_L(k, \theta) = -2\pi m \omega \frac{n_H}{n_C} \frac{\omega_p^2}{k^2} R_L(k) \int d^3\mathbf{p} \delta(\omega - \mathbf{k} \cdot \mathbf{v}) \mathbf{k} \cdot \frac{\partial f(\mathbf{p})}{\partial \mathbf{p}}. \quad (7)$$

Let p_L and p_T be the components of \mathbf{p} longitudinal and transverse to \mathbf{k} . Then we have

$$\begin{aligned} \delta(\omega - \mathbf{k} \cdot \mathbf{v}) &= \frac{m}{k} \left(\frac{k^2 c^2}{k^2 c^2 - \omega^2} \right)^{3/2} \left[1 + \left(\frac{p_T}{mc} \right)^2 \right]^{1/2} \times \\ &\times \delta \left(p_L - mc \left\{ \frac{\omega^2}{k^2 c^2 - \omega^2} \left[1 + \left(\frac{p_T}{mc} \right)^2 \right] \right\}^{1/2} \right). \end{aligned} \quad (8)$$

We introduce a parameter u and a *projected distribution* $F(u)$ by

$$F(u) = \int d^3\mathbf{p} \left[1 + \left(\frac{p_T}{mc} \right)^2 \right]^{1/2} \delta \left(p_L - mc \left\{ \frac{\omega^2}{k^2 c^2 - \omega^2} \left[1 + \left(\frac{p_T}{mc} \right)^2 \right] \right\}^{1/2} - u \right) f(\mathbf{p}). \quad (9)$$

Then (7) reduces to

$$\gamma_L(k, \theta) = -2\pi m^2 \omega \frac{n_H}{n_C} \frac{\omega_p^2}{k^2} R_L(k) \left(\frac{k^2 c^2}{k^2 c^2 - \omega^2} \right)^{3/2} \left. \frac{dF(u)}{du} \right|_{u=0}. \quad (10)$$

The expression (10) is a relativistic generalization of an expression derived by Jackson (1960). The non-relativistic result applies in the formal limit $c \rightarrow \infty$, which requires $k^2 c^2 \gg \omega^2$ here.

C. THE RESONANCE HYPERBOLOID

According to the δ -function in (8), the resonance condition $\omega - \mathbf{k} \cdot \mathbf{v} = 0$ may be represented by a surface

$$\left(\frac{k^2 c^2 - \omega^2}{\omega^2} \right) \left(\frac{p_L}{mc} \right)^2 - \left(\frac{p_T}{mc} \right)^2 = 1 \quad (11)$$

in momentum space. This is the equation for a hyperboloid of two sheets; only the sheet with $p_L > 0$ is physical.

A given hyperboloid has the smallest value of p_L at

$$(p_L)_{\min} = \left(\frac{\omega^2}{k^2 c^2 - \omega^2} \right)^{1/2} mc. \quad (12)$$

The asymptotic cone

$$p_T = \left(\frac{k^2 c^2 - \omega^2}{\omega^2} \right)^{1/2} p_L \quad (13)$$

has its apex at the origin and its axis along \mathbf{k} . An example of a *resonance hyperboloid* is illustrated in Figure 1.

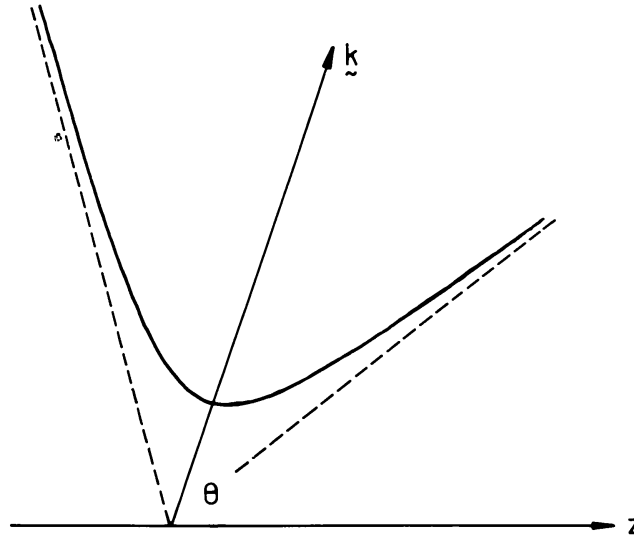


Fig. 1. A resonance hyperboloid in momentum space for a Langmuir wave. The propagation vector \mathbf{k} is an axis of symmetry for the surface and for its asymptotic cone (indicated by dashed lines).

In the non-relativistic limit, the resonance hyperboloid reduces to a plane at perpendicular distance $p_L = m\omega/k$ from the origin along \mathbf{k} . In this case (10) may be interpreted as follows: $F(u)$ is proportional to the number of particles on the plane $u = p_L - m\omega/k = 0$, and the condition for growth $dF(u)/du > 0$ at $u = 0$ corresponds to this number of particles increasing as the resonance plane moves away from the origin along \mathbf{k} .

The relativistic generalization of the foregoing condition for growth is as follows. Consider a set of nested resonance hyperboloids for a given direction \mathbf{k} . $F(u)$ is proportional to the number of particles on a given hyperboloid u , and the condition $dF(u)/du > 0$ at $u = 0$ requires that this number increase with increasing $(p_L)_{\min}$.

D. THE PROJECTED DISTRIBUTION

The projected distribution $F(u)$ defined by (9) may be reduced to a more useful form by introducing variables P , ψ , and ϕ in momentum space. We write

$$p_L = u + \left(\frac{\omega^2}{k^2 c^2 - \omega^2} \right)^{1/2} P \cosh \psi, \quad p_T = P \sinh \psi \quad (14a,b)$$

with ϕ the azimuthal angle between \mathbf{p} and the plane containing \mathbf{k} and the axis of symmetry. Writing $f(P, \psi, \phi)$ for $f(\mathbf{p})$ in the new variables, (9) becomes

$$F(u) = m^2 c^2 \int_0^{2\pi} d\phi \int_0^\infty d\psi \sinh \psi \cosh^2 \psi f(mc, \psi, \phi). \quad (15)$$

In the Appendix we use (10) with (15) to rederive the known results for a shell distribution with a double-sided loss cone. The shell distribution with $\Delta p_0 \ll p_0$ corresponds to

$$f(\mathbf{p}) = \frac{\Phi(\alpha)}{4\pi p_0^2 \Delta p_0}, \quad p_0 \leq p \leq p_0 + \Delta p_0 \quad (16)$$

$$= 0 \quad \text{otherwise,}$$

and a two sided loss-cone distribution corresponds to

$$\Phi(\alpha) = \frac{1}{\cos \alpha_0}, \quad \alpha_0 \leq \alpha \leq \pi - \alpha_0 \quad (17)$$

$$= 0 \quad \text{otherwise,}$$

where α is the angle between \mathbf{p} and the axis of symmetry. Explicit results for $\gamma_L(k, \theta)$ were derived for the limit $\Delta p_0 \rightarrow 0$ by Melrose and Stenhouse (1977), cf. also Melrose (1980b, pp. 146–154).

These results are rederived in the Appendix using a partly geometric argument. The geometry is illustrated in Figure 2; the distribution (16) with (17) is represented by a spherical shell in momentum space with two loss-cone holes. Four cases are relevant: the resonance hyperboloid (i) touches the inner surface of the shell, (ii) cuts the shell without passing through either hole, (iii) cuts the shell and passes through one hole but not the other, and (iv) cuts the shell and passes through both holes. Growth is possible only in cases (iii) and (iv).

Growth in the case of a shell distribution can be interpreted relatively easily because the projected distribution $F(u)$ is proportional to the length of the arc of intersection of the resonance hyperboloid and the shell. For a loss-cone distribution the length of this arc can increase with $(p_L)_{\min}$ only if the hyperboloid passes through one or both holes. For a more realistic p -distribution, the change in the number of particles with p tends to oppose growth for $\partial f(p)/\partial p < 0$. Even granted $\partial f(p)/\partial p > 0$ over some finite range of p , there must exist a region at large p where $\partial f(p)/\partial p$ is negative and it is known that for an isotropic distribution the net effect is damping and not growth. Hence the variation with p opposes any tendency to growth, and this effect is minimized if $\partial f(p)/\partial p$ is positive (a ‘gap’ distribution) or nearly zero (a ‘plateau’ distribution), e.g. Kuijpers (1974) and Robinson (1977), over a range of p .

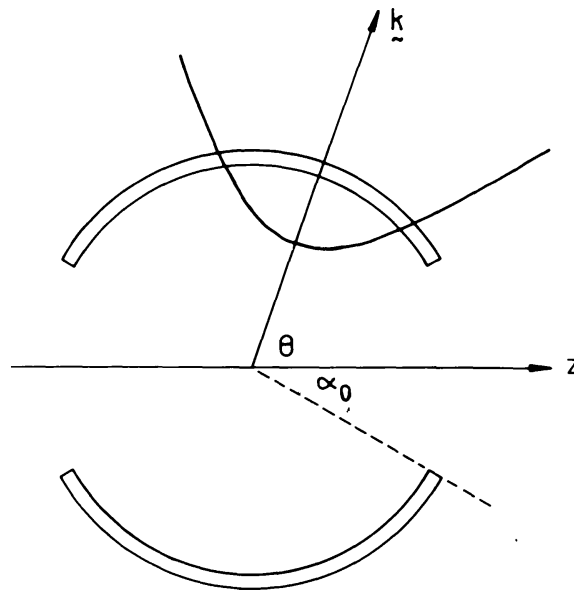


Fig. 2. The resonance condition for a spherical shell distribution in momentum space with two loss-cone holes. The resonant electrons lie on the surface of intersection of the shell with the resonance hyperboloid for the Langmuir wave.

3. Evolution of the Distribution Function

When a distribution of energetic particles is released in a magnetic trap, those with pitch angles in the loss cone precipitate and are lost in less than the particle traversal time along the trap. Thereafter the particle distribution evolves due to two effects of collisions, namely collisional slowing down and collisional scattering into the loss cone. We ignore non-collisional effects, and in particular we ignore the back reaction of the growth of Langmuir waves on the loss-cone distribution; this (so-called quasilinear relaxation) would cause an enhanced scattering into the loss cone and hence an enhanced rate of evolution of the distribution.

Benz and Kuijpers (1976) included only the effect of collisional slowing down, and found that the distribution evolves towards a plateau. The combined effect of slowing down and scattering into the loss cone leads to a gap distribution (Melrose and Brown, 1976). Scattering into the loss cone also implies that the loss cone is not entirely empty: rather than dropping sharply to zero at $\alpha = \alpha_0$ the pitch-angle distribution falls off over a range of $\Delta\alpha$ of order $(\tau_{sc}/\tau_{es})^{1/2}$ (Kennel, 1969), where τ_{sc} is the scattering time and τ_{es} is the escape time (\simeq half the traversal time).

It is desirable to explore the implications of such evolution on likely distributions, and to compare the resulting growth rates with those calculated assuming more idealized distributions.

A. TRAP PLUS PRECIPITATION MODEL

Let $\bar{f}(p, t)$ be the distribution function averaged over pitch angle. In the presence of collisions with a frequency $\sim (V/v)^3$, Melrose and Brown (1976) found that $\bar{f}(p, t)$

evolves according to

$$\bar{f}(p, t) = \left(\frac{v}{v_0}\right)^4 \bar{f}(p_0, 0) \quad (18)$$

with $p = mv$ here,

$$v_0 = v \left[1 + \frac{At}{v^3} \right]^{1/3}, \quad (19)$$

and where $\bar{f}(p, 0)$ is the distribution at $t = 0$. The parameter A in (19) is given by

$$\frac{A}{c^3} = 1.8 \times 10^{-18} n_C s^{-1} \quad (20)$$

with n_C per cubic meter.

(i) *Hot Maxwellian Distribution*

The evolution of a hot Maxwellian distribution is shown in Figure 3. The initial

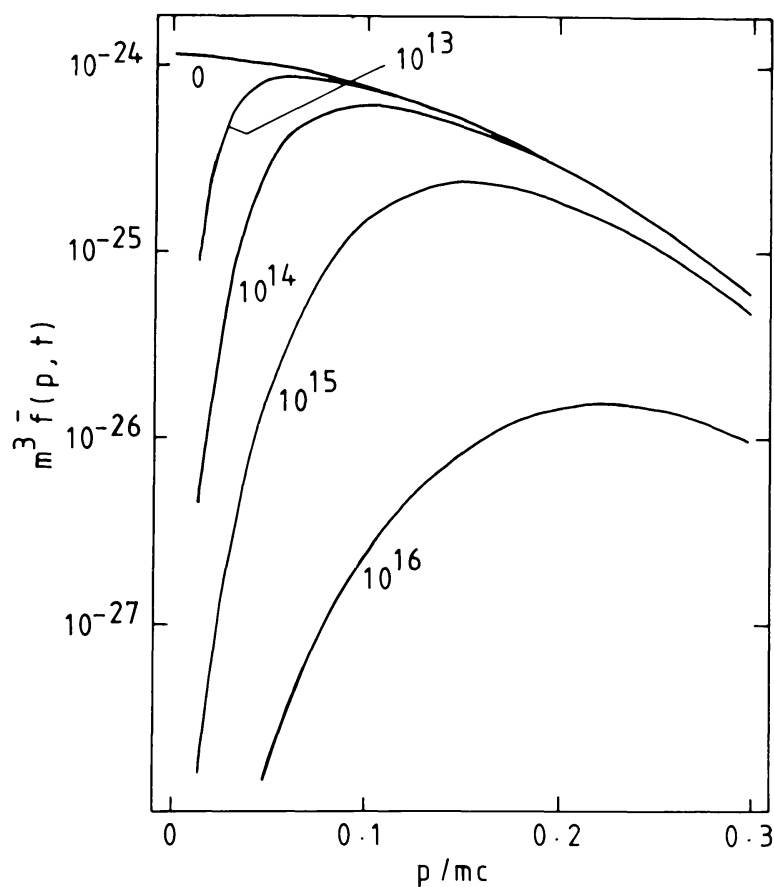


Fig. 3. The time evolution of a hot Maxwellian distribution with a single or double sided loss cone as a result of collisions with a relatively cold and dense background distribution. The initial temperature of the hot distribution is 10 keV. The sequence of curves showing the angle averaged distribution function in units of $m^{-6} s^3$ is labelled with the product $n_C t$ of the background number density n_C and time in units of $m^{-3} s$.

temperature is $T = 10$ keV corresponding to a thermal speed $V/c = 0.19$; we assume that $n_H/n_C \ll 1$. Time is parameterized by $n_C t$ and $m^3 \bar{f}(p, t)$ is plotted as a function of p/mc . A sharply rising ($\sim p^4$) part of the distribution develops and, as time elapses, the peak in the distribution moves to higher momenta. After about $n_C t = 10^{15} \text{ m}^{-3} \text{ s}$ the peak value of $\bar{f}(p, t)$ has dropped below its initial value by about an order of magnitude, and this decrease is by about two orders of magnitude for $n_C t = 10^{16} \text{ m}^{-3} \text{ s}$.

(ii) *Power-Law Distribution*

In Figure 4 we show the corresponding evolution for a power-law distribution

$$\begin{aligned} \bar{f}(p, 0) &= \frac{K}{4\pi} \frac{\alpha - 3}{p_L^3} \left(\frac{p_L}{p}\right)^\alpha, & p \geq p_L \\ &= 0, & p < p_L \end{aligned} \quad (21)$$

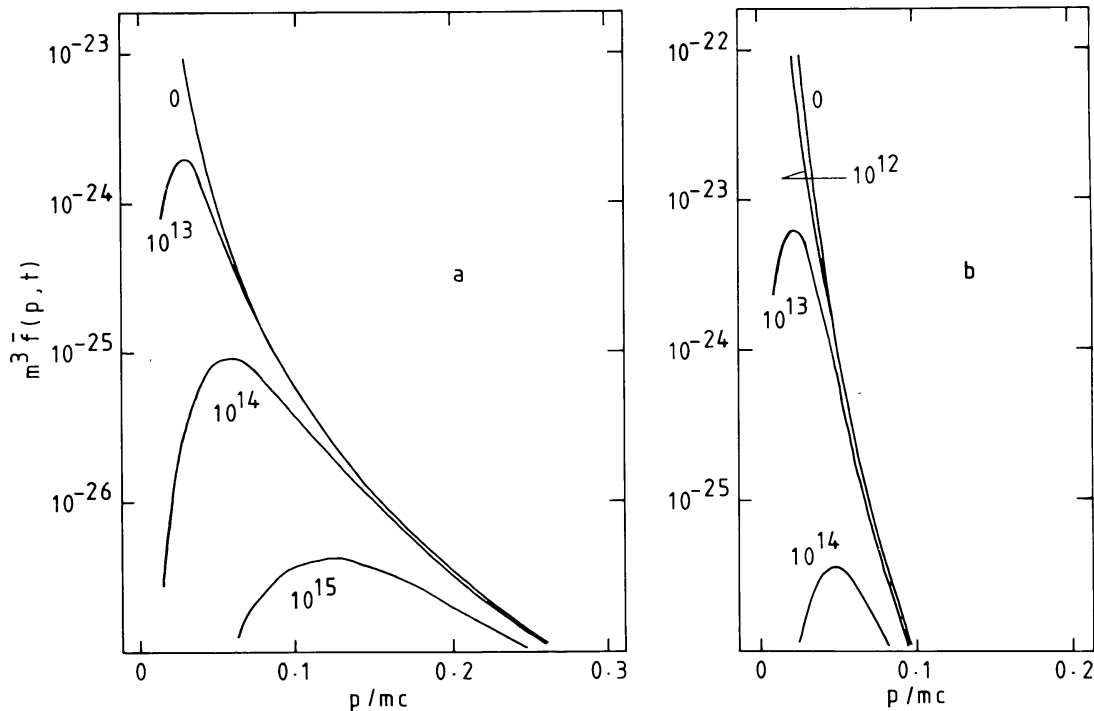


Fig. 4. As for figure 3 except for power-law distributions with (a) $\alpha = 4$ and (b) $\alpha = 7$. In each case the initial number density of the distribution is chosen so that the angle-averaged distribution function has the same value as that for the Maxwellian distribution of Figure 3 at $p/mc = 0.05$.

with $p_L/mc = 0.02$ and $\alpha = 4$ and 7 ; in both cases $\bar{f}(p, 0)$ is normalized so that $m^3 \bar{f}(p, 0)$ is equal to the value for a 10 keV Maxwellian at $p/mc = 0.05$. The number of particles drops much faster with time for the power law distribution than for the Maxwellian case, and this decrease becomes faster with increasing α .

B. NO SCATTERING INTO THE LOSS CONE

If collisional slowing down is included but collisional scattering into the loss cone is not, then the evolution is described by (18) without the factor $(v/v_0)^4$. This case was considered by Benz and Kuijpers (1976). We plot the evolution of an initial Maxwellian distribution in Figure 5. As found by Benz and Kuijpers (1976) such distributions evolve to a plateau.

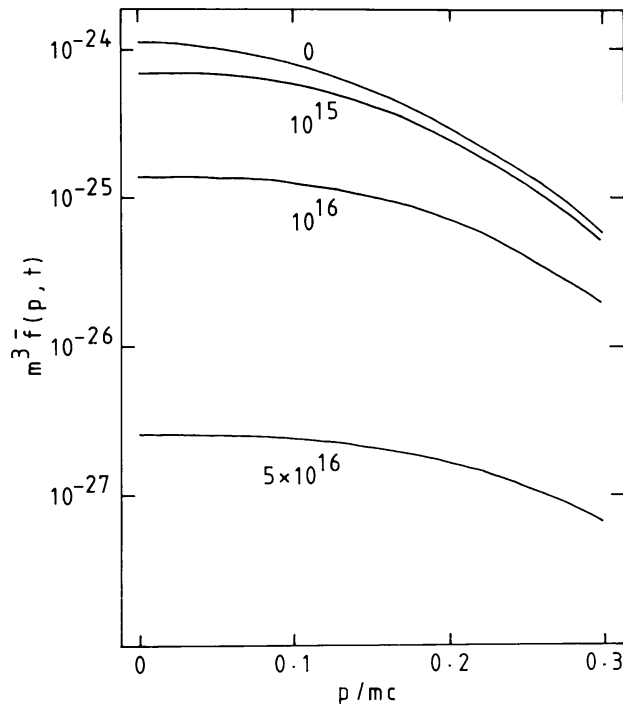


Fig. 5. As for Figure 3 except that the effect of collisional scattering into the loss cone is ignored. Note that the distribution evolves to a 'plateau' distribution rather than a 'gap' distribution.

This case is artificial when applied to a loss-cone distribution: escape is implicit in the assumption of a loss-cone anisotropy, but escape through scattering into the loss cone is not included in the evolution of $f(p, t)$. We include this case only to allow comparison between the 'gap' distributions, e.g. as in Figures 3 and 4, and the 'plateau' distribution of Figure 5.

4. Numerical Results

In our numerical calculations of the growth rate we have used (10) assuming a given form for the loss-cone distribution and determining $f(p, t)$ as discussed in Section 3. Our primary interest is in determining how the growth rate varies as a function of k and θ , and hence we plot curves of $\gamma_L(k, \theta)$ for given k and varying θ , with the k -values chosen to cover the range where growth occurs.

A. THE LOSS-CONE DISTRIBUTION

The loss-cone distribution is assumed to be either single sided or double sided, i.e. either a single hole at $\alpha \leq \alpha_0$ or holes at both $\alpha \leq \alpha_0$ and $\alpha \geq \pi - \alpha_0$. Inside the loss cones $\Phi(\alpha)$ is assumed to vary as (Hewitt *et al.*, 1982)

$$\Phi(\alpha) \sim \begin{cases} \left[\sin\left(\frac{\pi}{2} \frac{\alpha}{\alpha_0}\right) \right]^N, & \alpha \leq \alpha_0, \\ \left[\sin\left(\frac{\pi}{2} \frac{\pi - \alpha}{\alpha_0}\right) \right]^N, & \alpha \geq \pi - \alpha_0. \end{cases} \quad (22)$$

Growth is effective only for relatively large values of α_0 , and we usually choose $\alpha_0 = 30^\circ$ or 45° . The parameter N determines the sharpness with which the distribution drops towards zero inside the loss cone; we assume $N = 6$ except when examining the effect of changing N .

B. LANDAU DAMPING

Landau damping by the background electrons gives a negative contribution to the net growth rate. Rather than add this contribution, we calculate it separately and denote its values on the left-hand side of the plots of $\gamma_L(k, \theta)$. Since $\gamma_L(k, \theta)$ is proportional to the hot number density, n_H , this procedure enables growth rates for other values of n_H to be readily obtained from the information presented in the graphs. We ignore values of k where $\gamma_L(k, \theta)$ is always less in magnitude than the Landau damping coefficient (i.e. there is no net growth). Landau damping is sensitive to the assumed background temperature T_C ; we choose values of T_C ranging from 5×10^5 K to 2×10^6 K.

C. DOUBLE-SIDED LOSS-CONE DISTRIBUTION

The case which is most likely to be relevant to solar radio bursts is that of a double-sided loss-cone distribution in which $\bar{f}(p, t)$ evolves according to the trap-plus-precipitation model, cf. Section 3A. In all our calculations we assume $n_C = 1 \times 10^{15} \text{ m}^{-3}$, implying $\omega_p/2\pi = 300$ MHz.

In Figures 6 to 10 we plot results for an initial hot Maxwellian with $n_H = 1 \times 10^{13} \text{ m}^{-3}$, $T_H = 1 \times 10^8$ K for a sequence of times: 0 s, 0.01 s, 0.1 s, 1 s, and 10 s, respectively. In each case we assume $N = 6$, and plot a left-hand series for $\alpha_0 = 30^\circ$ and a right-hand series for $\alpha_0 = 45^\circ$ with the series having $T_C = 5 \times 10^5$ K, 1×10^6 K, and 2×10^6 K from top to bottom. The hot component causes damping rather than growth for values of k smaller than those shown on the respective graphs. In Figures 6 to 9 the graphs for those values of α_0 and T_C for which the hot component causes either damping or growth smaller than the Landau damping for all values of k and θ have been omitted. Thus, for example, when $t = 0$ s and 0.01 s growth is not possible for $\alpha_0 = 30^\circ$ for any of the three temperatures and for $\alpha_0 = 45^\circ$, the Landau damping is larger than the contribution to growth from the hot distribution when $T_C = 1 \times 10^6$ K and 2×10^6 K.

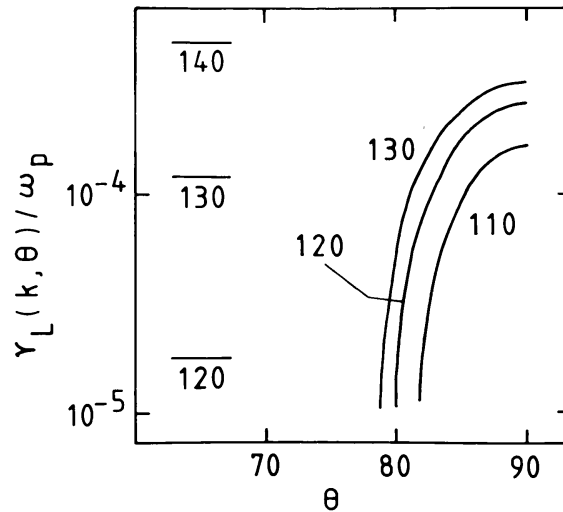


Fig. 6. The normalized growth rates for Langmuir waves γ_L/ω_p are plotted as a function of propagation angle θ in degrees for the indicated values of the wavenumber k in m^{-1} . The waves are generated by a hot Maxwellian distribution with a double-sided loss cone in the presence of a relatively cold and dense Maxwellian background distribution. The parameters for the hot distribution are $n_H = 1 \times 10^{13} \text{ m}^{-3}$, $T_H = 1 \times 10^8 \text{ K}$, $\alpha_0 = 45^\circ$ and $N = 6$ and those for the 'cold' distribution are $n_C = 1 \times 10^{15} \text{ m}^{-3}$ and $T_C = 5 \times 10^5 \text{ K}$. Damping rather than growth occurs for values of k smaller by 10 m^{-1} than those shown. The Landau damping due to the cold background is not included in the growth rate curves but shown separately on the left of the figure as horizontal lines labelled by the appropriate values of k . The Landau damping is larger than the contribution to growth from the hot distribution for values of k larger by 10 m^{-1} than those shown.

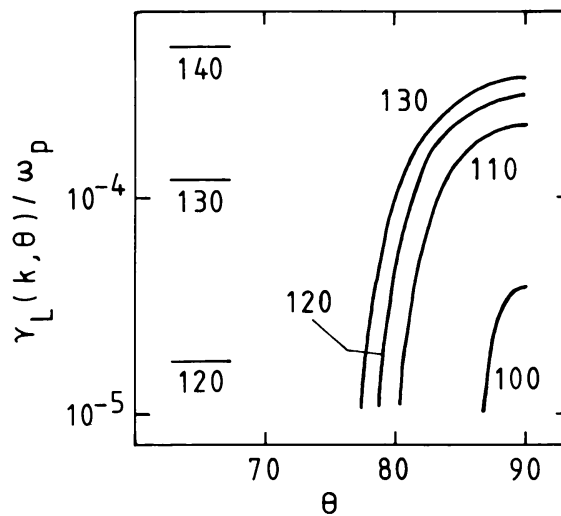


Fig. 7. As for Figure 6 except that the hot distribution has evolved for 0.01 s according to Equations (18) to (20).

The value of T_C affects not only the Landau damping but also the dispersion relation for Langmuir waves, cf. (3). Only the latter effect is included explicitly in the curves since the Landau damping is shown separately. As the size of the gap in the distribution function increases with time, the range of values of k for which net growth occurs

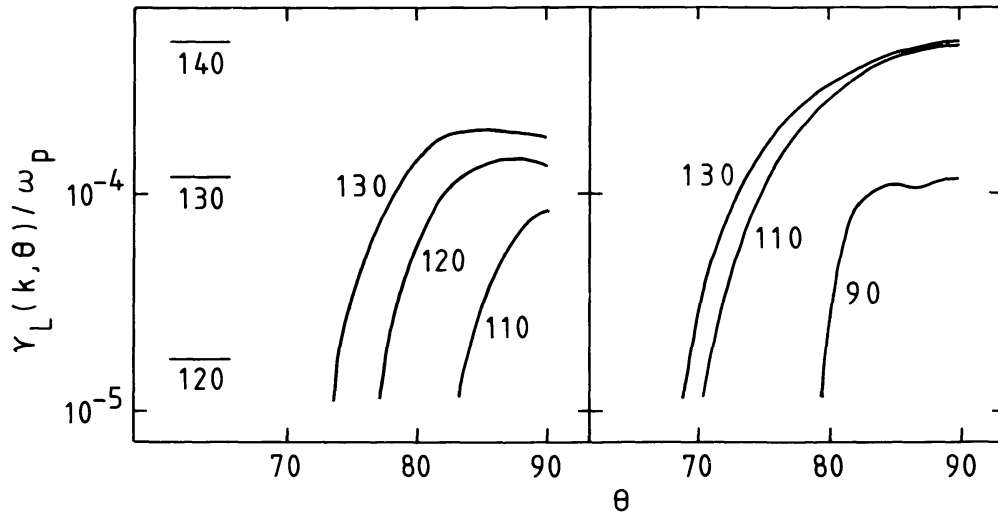


Fig. 8. As for Figure 6 except that the hot distributions have evolved for 0.1 s and $\alpha_0 = 30^\circ$ (left) and 45° (right).

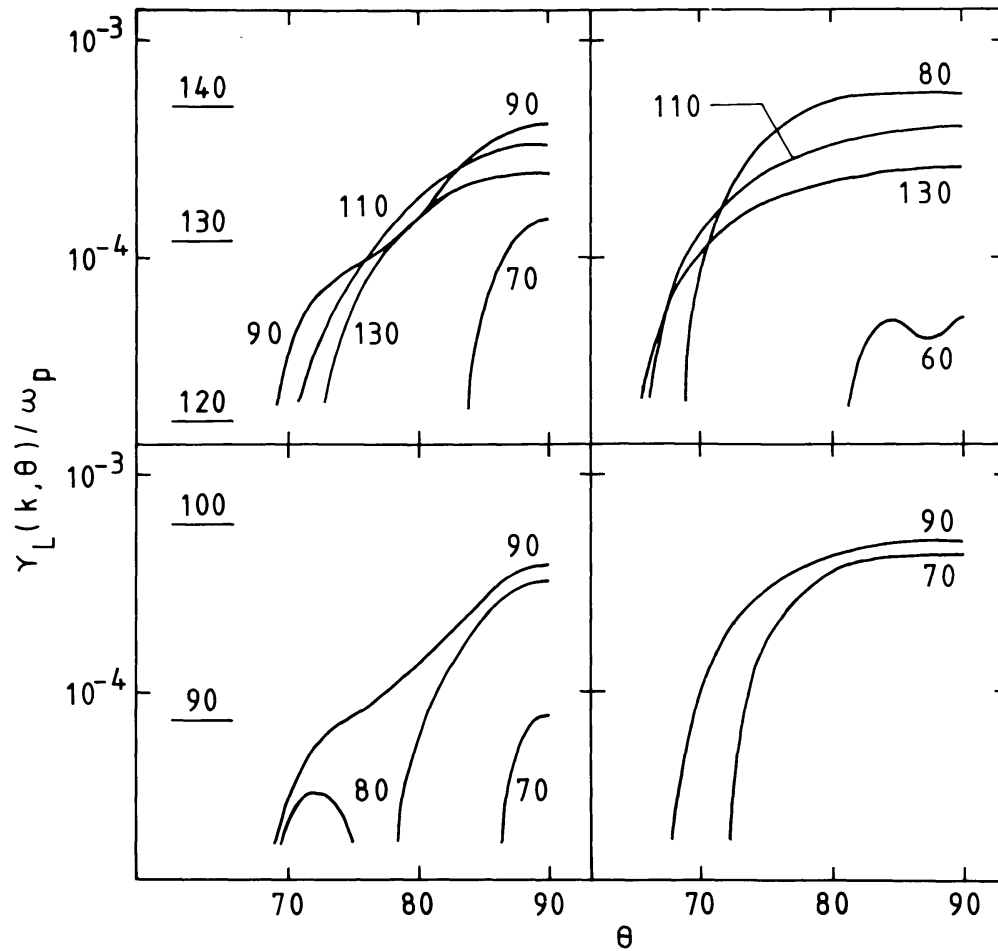


Fig. 9. As for Figure 6 except that the hot distributions have evolved for 1 s and $\alpha_0 = 30^\circ$ (left column) and 45° (right column) and $T_c = 5 \times 10^5$ K (top row) and 1×10^6 K (bottom row).

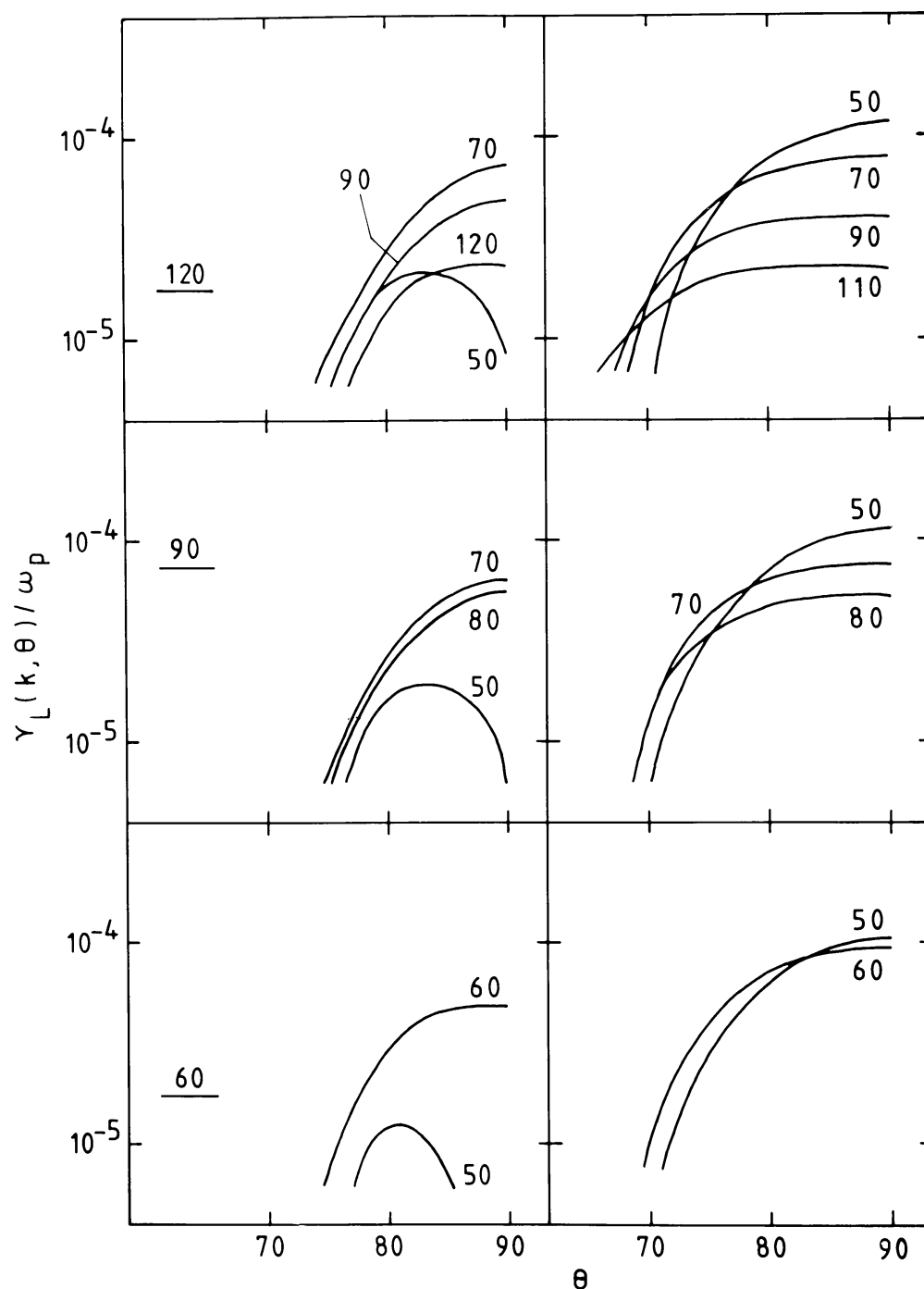


Fig. 10. As for Figure 6 except that the hot distributions have evolved for 10 s and $\alpha_0 = 30^\circ$ (left column) and 45° (right column) and $T_C = 5 \times 10^5$ K (top row), 1×10^6 K (middle row) and 2×10^6 K (bottom row).

increases and net growth is possible for higher values of the background temperature T_C . The growth rates, however, decrease rapidly after times $t \sim 1$ s since the number density of hot particles decreases significantly (cf. Figure 3).

The growth rate is a maximum at $\theta = 90^\circ$ except for low values of k , particularly for $\alpha_0 = 30^\circ$. The widths of the peaks around $\theta = 90^\circ$ are broader for $\alpha_0 = 45^\circ$ than for $\alpha_0 = 30^\circ$.

We have repeated these calculations for $N = 3$ rather than $N = 6$ in (22), i.e. for a less steep fall-off in the loss cone. The growth rates are systematically smaller, and for low values of k we find damping for $N = 3$ instead of the growth found for $N = 6$. An example is plotted in Figure 11 for which all parameters other than N are the same as those for the top row of Figure 10.

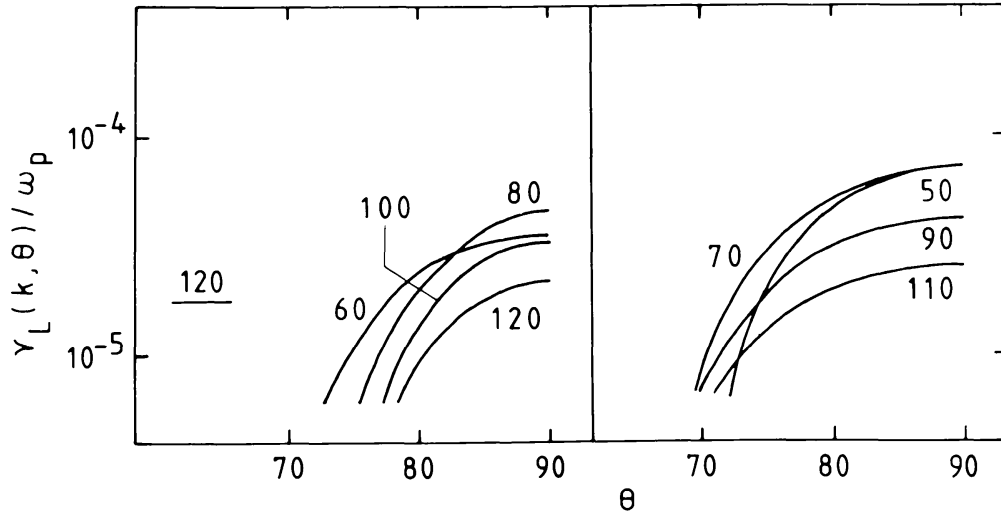


Fig. 11. As for the top row of Figure 10 except that $N = 3$.

We have also repeated the calculations for the power-law distributions shown in Figure 4. We find that no net growth is possible for $\alpha = 7$ (cf. (21)) under conditions similar to those for Figures 6 to 10. Net growth is possible in some cases for $\alpha = 4$. An example is plotted in Figure 12 for $\alpha_0 = 45^\circ$, $T_C = 5 \times 10^5$ K and other parameters similar to those in Figure 9. The growth rates for power-law distributions are systemati-

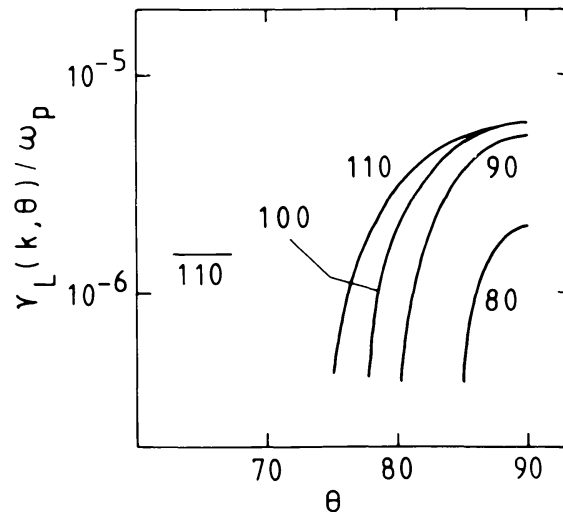


Fig. 12. As for Figure 6 except for an $\alpha = 4$ power-law distribution after 1 s evolution. The distribution is normalized as discussed below Equation (21).

cally less than those for a corresponding Maxwellian distribution. Note that in comparing the power-law and Maxwellian distributions there is an arbitrariness in the lower cutoff of the power-law distribution which we have removed by requiring that the distribution functions be equal at a specific momentum ($p/mc = 0.05$), cf. remarks following (21) above.

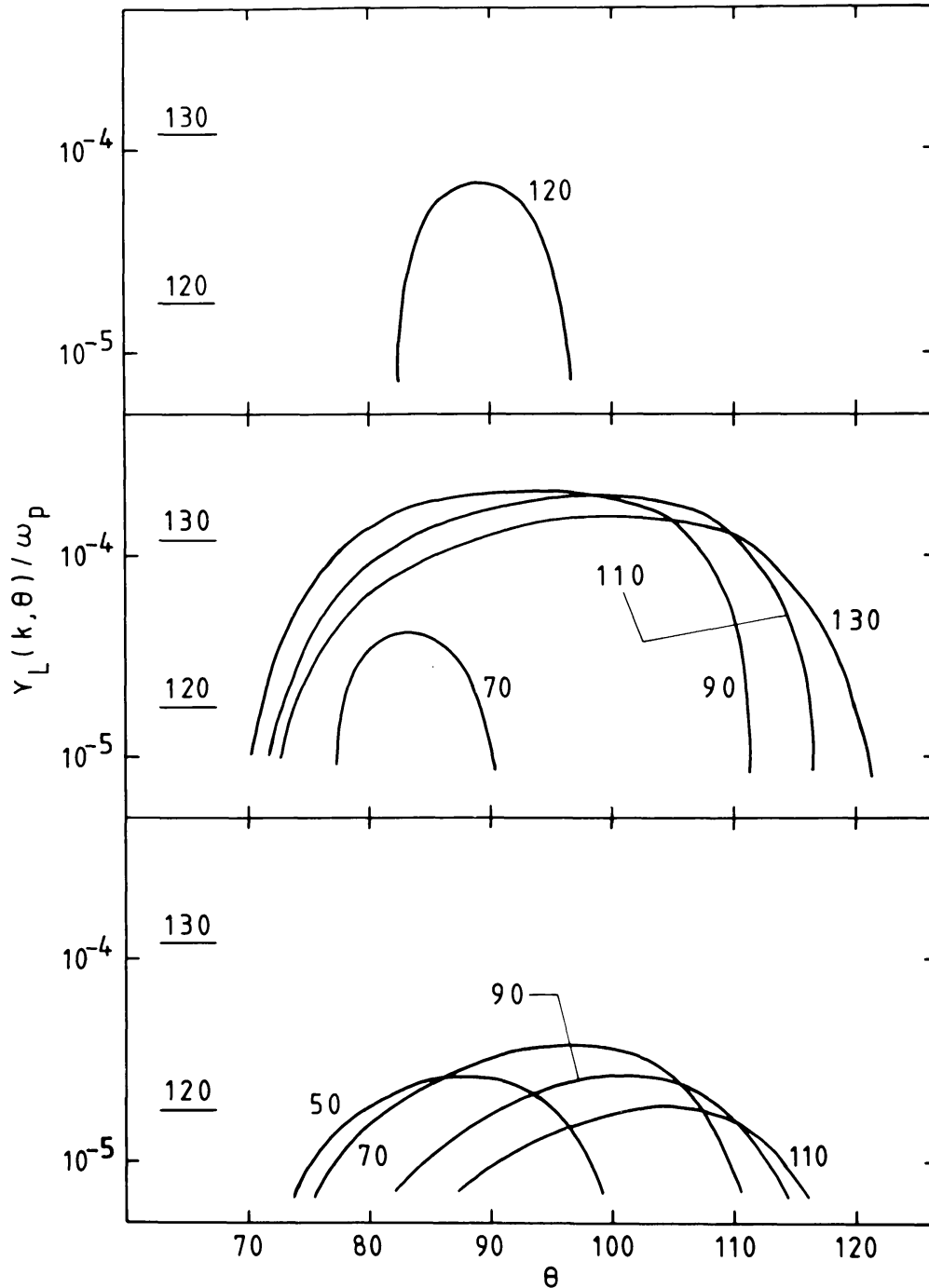


Fig. 13. As for Figure 6 except for a hot Maxwellian distribution with a single sided loss cone evolved for 0.1 s (top), 1 s (middle), and 10 s (bottom). The loss cone angle is 45° .

D. SINGLE-SIDED LOSS CONE

For comparison we have repeated the calculations of the growth rate for a hot Maxwellian assuming a single-sided loss-cone distribution at $\alpha \leq \alpha_0$. We fix $\alpha_0 = 45^\circ$ and $T_C = 5 \times 10^5$ K with the other parameters as in Figures 8 to 10, and plot the resulting growth rates for $t = 0.1$ s, 1 s and 10 s in Figure 13. An interesting effect is that for larger values of k the maximum growth occurs at $\theta > 90^\circ$.

E. COMPARISON WITH EXISTING RESULTS

Two difficulties prevented us from comparing our numerical results in detail with the primarily analytic results of Zaitsev and Stepanov (1983). Firstly, these authors assumed a Maxwellian with a sharply cut off pitch-angle distribution whereas our numerical code requires a smoothly varying pitch-angle distribution. This difficulty is not a serious one in practice because the growth rates do not vary rapidly with increasing N , cf. (22), and our results for large N should be reasonable approximations to those for a sharp loss cone. The second difficulty arose from the formula for the growth rate used by Zaitsev and Stepanov, cf. their (6), and attributed by them to Korablev (1967) and Trakhtengertz (1968). In fact Korablev and Trakhtengertz gave different results, with Korablev's containing an extra term; Zaitsev and Stepanov used Trakhtengertz' formula. We have checked the derivation and find that a term is indeed missing from Trakhtengertz' formula, but we have not been able to show that this term reduces to the form quoted by Korablev. Zaitsev and Stepanov's omission of this term led them to systematically overestimate the growth rate. Nevertheless on comparing (a) Zaitsev and Stepanov's result, (b) the corrected form of their result, and (c) the corresponding result using our code with $N = 6$, we found that the maximum growth rates differed by no more than a factor of two.

Benz and Kuijpers (1976) found growth rates for an initial $\alpha = 7$ power-law distribution with a loss cone. As pointed out in Section 3B above, they made the artificial assumption of evolution without any scattering into the loss cone. As a consequence, their results are several orders of magnitude smaller than those found here. This is primarily due to the fact that when scattering into the loss cone is neglected the distribution evolves to a 'plateau' rather than a 'gap'. In addition their initial power-law distribution is relatively soft and by the time a plateau has formed, the number of energetic electrons has decreased considerably from its initial value.

We conclude that there is no obvious inconsistency between our results and these earlier ones.

5. Discussion and Conclusions

Although growth of Langmuir waves is possible for a variety of loss-cone distributions, a clear indication arises from our results that growth is most favorable under quite specific conditions:

- (i) The loss cone needs to be of intermediate size, e.g. $\alpha_0 \sim 45^\circ$. (Our growth rates

increase with the size of the loss cone for fixed n_H/n_C . In a coronal loop, the ratio n_H/n_C decreases with increasing loss cone angle.)

(ii) The pitch-angle distribution needs to fall off relatively sharply inside the loss cone.

(iii) The suprathermal particles need to have a 'gap' distribution, i.e. a region with $\partial f(p)/\partial p > 0$.

(iv) The initial suprathermal distribution (assuming the gap forms as in a trap-plus-precipitation model) needs to be reasonably dense and relatively hard, e.g. a hot Maxwellian or a power law $f(p) \sim p^{-\alpha}$ with $\alpha \lesssim 4$. (Otherwise the relative number of particles above the gap is small and only these particles drive the instability.)

(v) The background electrons need to be relatively cool. (Otherwise Landau damping by them precludes any growth.)

Granted that these conditions are satisfied, our results show that the growth rate can be as high as 0.05 times $(n_H/n_C)\omega_p$, where n_H refers to the initial number density of the suprathermal electrons.

The size of the loss cone, i.e. α_0 , in an idealized trap varies from a minimum value $(\alpha_0)_{\min} = \arcsin(B_{\min}/B_{\max})^{1/2}$ at the point $B = B_{\min}$ where the field is weakest to $\alpha_0 = 90^\circ$ at $B = B_{\max}$ where the electrons escape. However on the Sun most particles are lost only when they enter a region where the electron density is such that a collisional mean free path for the particle is roughly a scale height. Let $B = B_{\max}$ be identified as this point. It is clear that the loss cone cannot be sharply defined near $B = B_{\max}$ because there the particles are strongly scattered. Hence one expects a relatively sharp large loss cone, at $\alpha_0 = 45^\circ$ say, only if the altitude where $B = B_{\max}/2$ lies at least several scale heights above the altitude where $B = B_{\max}$. The point is that collisions in the denser regions produce a relatively high albedo which should smear out the loss cone anisotropy near $B = B_{\max}$. To our knowledge no detailed investigation of the effects of this albedo has been made, and such an investigation is desirable. We expect an optimum region for growth where the tendency of α_0 to increase with decreasing height (favoring growth) is offset by the increasing smearing of the edges of the loss cone with decreasing height.

The formation of a 'gap' is a transitory process requiring an injection (or acceleration) of electrons in the trap which terminates at some time, t_0 say. The 'gap' develops and remains only for a few collision times before most of the particles precipitate. (Any further injection or acceleration can fill the 'gap' and suppress the growth, in a similar fashion to that envisaged by Benz and Kuijpers (1976).) Assuming suprathermal electrons with mean energies ~ 10 keV, the typical timescale is of order $10^5/f_p^2$ seconds, where f_p is in megahertz. In any suggested application one would expect this characteristic timescale to play an important role. For microwave emission from flare kernels (Zaitsev and Stepanov, 1983) and for features in decimetric type IV continua (Kuijpers, 1980) this time scale is a reasonable one; for type I emission it is intermediate between the time scales of type I bursts and of variations in the type I continuum.

Besides this characteristic time scale, there are two other features which one would predict for plasma emission arising from loss-cone driven Langmuir waves. The Langmuir waves are emitted preferentially perpendicular to the magnetic field lines and hence they can coalesce to produce second harmonic plasma emission without any

intermediate scattering into the backward direction, as required for Langmuir waves driven by a streaming instability. The two features are that one expects (a) second harmonic plasma emission, (b) which is weakly polarized in the sense of the x -mode (Melrose *et al.*, 1978, 1980).

The conditions required for the loss-cone instability to develop do not seem at all severe. A relatively hard spectrum of electrons needs to be injected into the trap; although earlier data (e.g. Lin, 1974) suggested relatively soft spectra ($\alpha \sim 7$ in (21)) for escaping electrons with energies $\gtrsim 10$ keV, more recent data are consistent with harder power-law or Maxwellian spectra for suprathermal electrons at $\lesssim 10$ keV, e.g. Lin *et al.* (1981). It seems plausible that some electrons would enter magnetic loops and be trapped for long enough for the loss-cone instability to become effective. This plausibility argument complements the one given in the Introduction that loss-cone driven Langmuir turbulence is a plausible mechanism for a variety of solar radio bursts. However, interpretation of specific phenomena in terms of this mechanism remains at a rudimentary level and further detailed investigation is required.

Finally we comment on two related formal points. First, the concept of a resonance hyperboloid, cf. Section 2C, provides a powerful tool for analysing the growth rate. We have not emphasized this point because we have used this tool only to rederive known results (cf. Appendix). Second, the concepts of a resonance hyperboloid in the unmagnetized case and of a resonance ellipse in the magnetized case (e.g. Hewitt *et al.*, 1982) should be related in some sense, e.g. in the limit of weak magnetic field. However, this relation is evidently a subtle one: in practice there is a dichotomy in the treatment of the magnetized and unmagnetized cases, and we have not been successful in rectifying this. Consequently we have not commented at all on the magnetized case in this paper.

Acknowledgements

One of us (RGH) wishes to acknowledge the hospitality of the Department of Astrophysical, Planetary and Atmospheric Sciences at the University of Colorado where this work was commenced.

Appendix: Shell Distribution with a Double-Sided Loss Cone

The absorption coefficient for the shell distribution (16) with (17) was evaluated in the limit $\Delta p_0 \rightarrow 0$ by Melrose and Stenhouse (1977) and quoted by Melrose (1980b, p. 147):

$$\gamma_L(k, \theta) = \gamma_L^I(k, \theta) + \gamma_L^R(k, \theta) + \gamma_L^A(k, \theta), \quad (\text{A.1})$$

$$\gamma_L^I(k, \theta) = \frac{\pi}{2} \frac{n_H}{n_C} \omega_p m v_0 \delta(p_0 - p_\phi) \Phi(\theta), \quad (\text{A.2a})$$

$$\gamma_L^R(k, \theta) = \frac{\pi}{2} \frac{n_H}{n_C} \omega_p \frac{2m v_\phi^3}{p_0 c^2} g(\theta, \chi), \quad (\text{A.2b})$$

$$\gamma_{\perp}^A(k, \theta) = -\frac{\pi}{2} \frac{n_H}{n_C} \omega_p \frac{m^3 v_{\phi}^2 v_0}{p_0^3} \{1 + (\gamma_0^2 - 1) \sin^2 \chi\} \frac{\partial g(\theta, \chi)}{\partial \cos \chi} \quad (\text{A.2c})$$

with $v_{\phi} = \omega/k$, $p_{\phi} = \gamma_{\phi} m v_{\phi}$, $\gamma_{\phi} = (1 - v_{\phi}^2/c^2)^{-1/2}$, $p_0 = \gamma_0 m v_0$, $\gamma_0 = (1 - v_0^2/c^2)^{-1/2}$, $\chi = \arccos(v_{\phi}/v_0)$ and

$$g(\theta, \chi) = \frac{1}{\pi} \int_{\cos(\theta+\chi)}^{\cos(\theta-\chi)} d \cos \alpha \frac{\Phi(\alpha)}{\{1 + 2 \cos \alpha \cos \theta \cos \chi - \cos^2 \alpha - \cos^2 \theta - \cos^2 \chi\}^{1/2}}. \quad (\text{A.3})$$

The resonance hyperboloid intersects the shell on a ring. In the limit $\Delta p_0 \rightarrow 0$ this ring becomes a circle of radius $p_0 \sin \chi$, a perpendicular distance $p_0 \cos \chi$ from the origin. The geometry is illustrated in Figure 14. The azimuthal angle ϕ introduced in (14a, b)

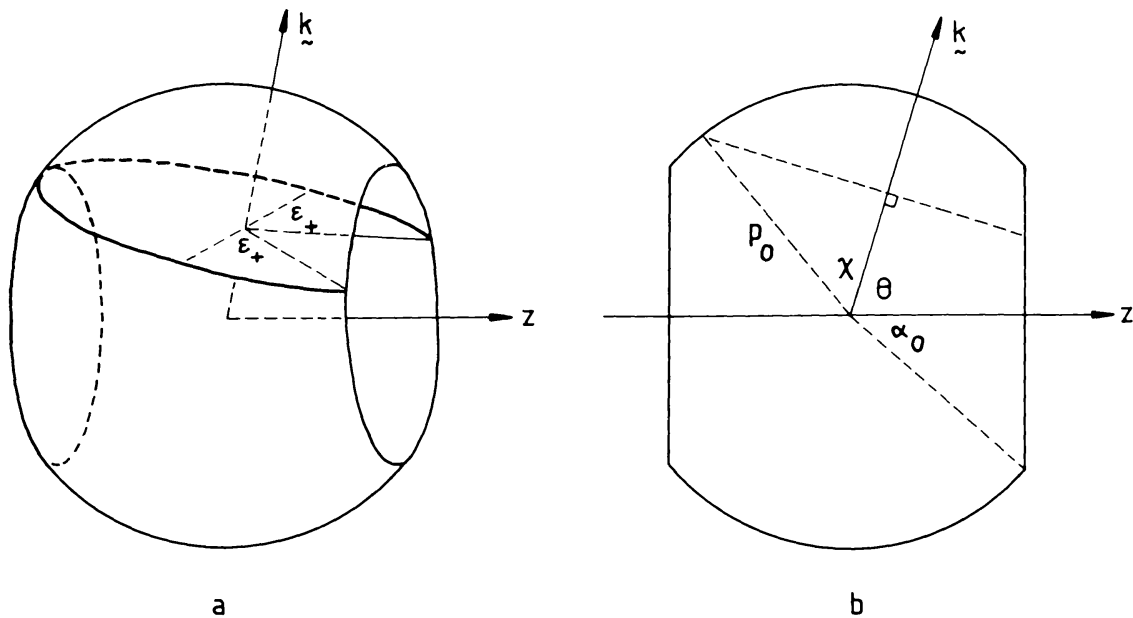


Fig. 14. The geometry of the ring of intersection of a resonance hyperboloid with a thin spherical shell containing two loss-cone holes. In (a) the hyperboloid just grazes the edge of one of the holes and passes through the other. For this value of k and for values of θ less than this critical angle, the angle subtended by the ring of intersection at its center is $\pi + 2\epsilon_+$. The angle ϵ_+ is defined by (A.4) in terms of the angles θ , α_0 , χ indicated in (b) which shows a section in the plane containing \mathbf{k} and the axis of symmetry.

may be identified as the angle subtended by a point on the ring relative to the center of the ring. If the hyperboloid does not pass through either loss-cone hole then ϕ ranges from 0 to 2π . More generally, let us define the angles

$$\epsilon_{\pm} = \arcsin \left\{ \frac{\cos \alpha_0 \mp \cos \theta \cos \chi}{\sin \theta \sin \chi} \right\}; \quad (\text{A.4})$$

these are real when the hyperboloid passes through one loss-cone hole (ε_+ real) or both loss-cone holes (ε_+ and ε_- both real). Then the total range of ϕ is

$$\begin{aligned} & 2\pi && \text{no hole ,} \\ \Delta\phi = & \pi + 2\varepsilon_+ && \text{one hole ,} \\ & 2\varepsilon_- + 2\varepsilon_+ && \text{two holes .} \end{aligned} \quad (\text{A.5})$$

The evaluation of $F(u)$, for small u , using (15) involves an integral over ϕ , which gives $\Delta\phi$, and an integral over ψ . Let $\psi = \psi_0$ and $\psi = \psi_0 + \Delta\psi_0$ correspond to the inner and outer surfaces of the shell. They are found from, cf. (14a, b) for $P = mc$,

$$\cosh \psi = \frac{\gamma}{\gamma_\phi} - \frac{uv_\phi}{mc^2\gamma_\phi} + 0(u^2) \quad (\text{A.6})$$

by setting $p = p_0$ and $p = p_0 + \Delta p_0$. Then (15) gives

$$F(u) = \frac{m^2c^2\Delta\phi}{12\pi p_0^2\Delta p_0 \cos \alpha_0} \{ \cosh^3(\psi_0 + \Delta\psi_0) - \cosh^3 \psi_0 \} + 0(u^2). \quad (\text{A.7})$$

The derivative with respect to u involves not only the hyperbolic functions

$$\frac{d}{du} \cosh \psi|_{u=0} = -\frac{v_\phi}{mc^2\gamma_\phi}, \quad (\text{A.8})$$

but also the angles ε_\pm in $\Delta\phi$:

$$\frac{d\varepsilon_\pm}{d \cos \chi} = \frac{\mp \cos \theta + \cos \alpha_0 \cos \chi}{\sin^2 \chi F_\pm(\alpha_0, \theta, \chi)}, \quad (\text{A.9})$$

$$F_\pm(\alpha, \theta, \chi) = [1 - \cos^2 \alpha - \cos^2 \theta - \cos^2 \chi \pm 2 \cos \alpha \cos \theta \cos \chi]^{1/2}, \quad (\text{A.10})$$

with $p_0 \cos \chi$ equal to p_L , i.e.

$$p_0 \cos \chi = m\gamma_0 v_\phi + \frac{u}{\gamma_\phi^2} + 0(u^2), \quad (\text{A.11})$$

and hence

$$\left. \frac{d \cos \chi}{du} \right|_{u=0} = \frac{1}{p_0 \gamma_\phi^2}. \quad (\text{A.12})$$

Now we consider each of the four cases listed in Section 2D separately.

Case (i): The hyperboloid touching the inner surface of the shell and not passing through either hole imply $p_\phi = p_0$ and $\Delta\phi = 2\pi$, respectively. Then with $\psi_0 = 0$ one finds to

lowest order in Δp_0

$$\left. \frac{dF(u)}{du} \right|_{u=0} = - \frac{mv_\phi \gamma_\phi^{-3} \gamma_0^2}{2p_0^2 \Delta p_0 \cos \alpha_0} \quad (\text{A.13})$$

and hence, from (15) with $p_\phi = p_0$, $v_\phi = v_0$, $\gamma_\phi = \gamma_0$,

$$\gamma_L(k, \theta) = \frac{\pi}{2} \frac{n_H}{n_C} \frac{m\omega v_0}{\Delta p_0 \cos \alpha_0}. \quad (\text{A.14})$$

(A.14) reproduces (A.2a) in the limit $\Delta p_0 \rightarrow 0$ with $p_0 = p_\phi$; in this limit one needs to reinterpret $1/\Delta p_0$ as $\delta(p_0 - p_\phi)$. The result applies only for $\alpha_0 < \theta < \pi - \alpha_0$ because otherwise the hyperboloid touches the surface $p = p_0$ only in the loss-cone holes, cf. Figure 14.

Case (ii): This is similar to Case (i) but with $p_0 > p_\phi$ so that the hyperboloid intersects the shell in a ring. Both $\psi_0 + \Delta\psi_0$ and ψ_0 are non-zero, and (A.7) with (A.6) and with $\Delta\phi = 2\pi$ implies

$$\left. \frac{dF(u)}{du} \right|_{u=0} = - \frac{\gamma_\phi^{-3} v_\phi}{p_0 m c^2 \cos \alpha_0} + 0(\Delta p_0), \quad (\text{A.15})$$

and (15) gives

$$\gamma_L(k, \theta) = \frac{\pi}{2} \frac{n_H}{n_C} \omega \frac{2mv_\phi^3}{p_0 c^2 \cos \alpha_0}. \quad (\text{A.16})$$

(A.16) reproduces (A.2b) for $g(\theta, \chi) = 1/\cos \alpha_0$, which applies for $\alpha_0 < \theta < \pi - \alpha_0$.

Case (iii): This is similar to Case (ii) except that the ring now passes through one of the holes in the shell, and this part of the ring is to be excluded in evaluating $\Delta\phi$, giving $\Delta\phi = \pi + 2\varepsilon_+$. Then one finds

$$\begin{aligned} \left. \frac{dF(u)}{du} \right|_{u=0} = & \frac{\gamma_\phi^{-3}}{2p_0 \cos \alpha_0} \left\{ - \frac{2v_\phi}{mc^2} \left[\frac{1}{2} + \frac{\varepsilon_+}{\pi} \right] + \right. \\ & \left. + \frac{\gamma_0 \gamma_\phi^{-2}}{\pi p_0} \left[\frac{-\cos \theta + \cos \alpha \cos \chi}{\sin^2 \chi F_+(\alpha_0, \theta, \chi)} \right] \right\}, \end{aligned} \quad (\text{A.17})$$

and hence

$$\begin{aligned} \gamma_L(k, \theta) = & \frac{\pi}{2} \frac{n_H}{n_C} \omega \frac{2mv_\phi^3}{p_0 c^2 \cos \alpha_0} \left\{ \left[\frac{1}{2} + \frac{\varepsilon_+}{\pi} \right] - \right. \\ & \left. - \frac{1}{2} \frac{c^2}{\gamma_\phi^2 v_0 v_\phi} \left[\frac{-\cos \theta + \cos \alpha \cos \chi}{\pi \sin^2 \chi F_+(\alpha_0, \theta, \chi)} \right] \right\}. \end{aligned} \quad (\text{A.18})$$

This reproduces (A.2b and c) when one takes account of $\gamma_0^2/\gamma_\phi^2 = 1 + (\gamma_0^2 - 1) \sin^2 \chi$ and of the explicit expression for $g(\theta, \chi)$, cf. Melrose (1980b, p. 153).

Case (iv): With the ring passing through both holes (A.18) is replaced by

$$\gamma_L(k, \theta) = \frac{\pi}{2} \frac{n_H}{n_C} \omega \frac{2mv_\phi^3}{p_0 c^2 \cos \alpha_0} \left\{ \frac{\varepsilon_-}{\pi} + \frac{\varepsilon_+}{\pi} - \frac{1}{2} \frac{c^2}{\gamma_\phi^2 v_0 v_\phi} \times \right. \\ \left. \times \left[\frac{-\cos \theta + \cos \alpha_0 \cos \chi}{\pi \sin^2 \chi F_-(\alpha_0, \theta, \chi)} + \frac{-\cos \theta + \cos \alpha_0 \cos \chi}{\pi \sin^2 \chi F_+(\alpha_0, \theta, \chi)} \right] \right\}, \quad (\text{A.19})$$

which again reproduces (A.2.b and c) when (10.75a, b) of Melrose (1980b, p. 153) is taken into account.

References

- Benz, A. O. and Kuijpers, J.: 1976, *Solar Phys.* **46**, 275.
 Benz, A. O. and Wentzel, D. G.: 1981, *Astron. Astrophys.* **94**, 100.
 Hewitt, R. G., Melrose, D. B., and Rönmark, K. G.: 1982, *Australian J. Phys.* **35**, 447.
 Jackson, J. D.: 1960, *J. Nuclear Energy C1*, 171
 Kennel, C. F.: 1969, *Rev. Geophys. Space Phys.* **7**, 379.
 Korabiev, A. V.: 1967, *JETP Letters* **5**, 111.
 Kuijpers, J.: 1974, *Solar Phys.* **36**, 157.
 Kuijpers, J.: 1980, in M. R. Kundu and T. E. Gergely (eds.), 'Radio Physics of the Sun', *IAU Symp.* **86**, 341.
 Lin, R. P.: 1976, *Space Sci. Rev.* **16**, 189.
 Lin, R. P., Schwartz, R. A., Pelling, R. M., and Harley, K. C.: 1981, *Astrophys. J.* **251**, L109.
 Melrose, D. B.: 1975, *Solar Phys.* **43**, 211.
 Melrose, D. B.: 1978, *Radiophys. Quantum Electron.* **20**, 945.
 Melrose, D. B.: 1980a, *Plasma Astrophysics*, Vol. I, Gordon and Breach, New York.
 Melrose, D. B.: 1980b, *Plasma Astrophysics*, Vol. II, Gordon and Breach, New York.
 Melrose, D. B.: 1980c, *Solar Phys.* **67**, 357.
 Melrose, D. B. and Brown, J. C.: 1976, *Monthly Notices Roy. Astron. Soc.* **176**, 15.
 Melrose, D. B., Dulk, G. A., and Gary, D. E.: 1980, *Proc. Astron. Soc. Australia* **4**, 50.
 Melrose, D. B., Dulk, G. A., and Smerd, S. F.: 1978, *Astron. Astrophys.* **66**, 315.
 Melrose, D. B. and Stenhouse, J. E.: 1977, *Australian J. Phys.* **30**, 481.
 Robinson, R. D.: 1977, dissertation, University of Colorado.
 Stepanov, A. V.: 1973, *Soviet Astron. A.J.* **17**, 781.
 Stepanov, A. V.: 1978, *Soviet Astron. Letters* **4**, 103.
 Tidman, D. A. and Dupree, T. H.: 1965, *Phys. Fluids* **8**, 1860.
 Trakhtengertz, V. Yu.: 1968, *Geomag. Aeron.* **8**, 263.
 Zaitsev, V. V. and Stepanov, A. V.: 1975, *Astron. Astrophys.* **45**, 135.
 Zaitsev, V. V. and Stepanov, A. V.: 1983, *Solar Phys.* **88**, 297.
 Zheleznyakov, V. V. and Zlotnik, E. Ya.: 1975, *Solar Phys.* **43**, 431.